Anti-malarial lead optimization studies on a 2,6-imidazopyridine series within a constrained chemical space to circumvent atypical dose-response curves against multi-drug resistant parasite strains.

Journal:	*Journal of Medicinal Chemistry*
Manuscript ID	jm-2018-013337.R1
Manuscript Type:	Article
Date Submitted by the Author:	21-Sep-2018

Complete List of Authors:	Le Manach, Claire; Drug Discovery and Development Center (H3D) Paquet, Tanya; University of Cape Town, Drug Discovery and Development Center (H3D) Wicht, Kathryn; university of Cape Town, Drug Discovery and Development Center (H3D) Nchinda, Aloysius; University of Cape Town, Drug Discovery and Development Center (H3D) Brunschwig, Christel; Division of clinical pharmacolgy, Drug Discovery and Development Center (H3D) Njoroge, Mathew; Division of clinical pharmacolgy, Drug Discovery and Development Center (H3D) Gibhard, Liezl; Division of clinical pharmacolgy, Drug Discovery and Development Center (H3D) Taylor, Dale; Division of clinical pharmacolgy, Drug Discovery and Development Center (H3D) Lawrence, Nina; Division of clinical pharmacolgy, Drug Discovery and Development Center (H3D) Wittlin, Sergio ; Schweizerisches Tropen- und Public Health-Institut Eyermann, Charles; University of Cape Town, Drug Discovery and Development Center (H3D) Basarab, Gregory; University of Cape Town, Department of Chemistry Duffy, James; Medicine for Malaria Venture Fish, Paul; University College London, ARUK UCL Drug Discovery Institute Street, Leslie; University of Cape Town, Drug Discovery and Development Center (H3D) Chibale, Kelly; University of Cape Town, Department of Chemistry

Anti-malarial lead optimization studies on a 2,6-imidazopyridine series within a constrained chemical space to circumvent atypical dose-response curves against multi-drug resistant parasite strains.

Claire Le Manach[†], Tanya Paquet[†], Kathryn Wicht[†], Aloysius T. Nchinda[†], Christel Brunschwig[∞], Mathew Njoroge[∞], Liezl Gibhard[∞], Dale Taylor[∞], Nina Lawrence[∞], Sergio Wittlin[◊,∫], Charles J. Eyermann[†], Gregory S. Basarab[†], James Duffy[‡], Paul V. Fish[ζ,þ], Leslie J. Street[†], and Kelly Chibale[,†,#]*

[†]Drug Discovery and Development Center (H3D), Department of Chemistry, University of Cape Town, Rondebosch 7701, South Africa; [∞]H3D, Division of Clinical Pharmacology, Department of Medicine, University of Cape Town, Observatory, 7925, South Africa; [◊]Swiss Tropical and Public Health Institute, Socinstrasse 57, 4002 Basel, Switzerland; [∫]University of Basel, 4003 Basel, Switzerland; [‡]Medicines for Malaria Venture, ICC, Route de Pré-Bois 20, PO Box 1826, 1215 Geneva, Switzerland; [ζ] Alzheimer's Research UK UCL Drug Discovery Institute, The Cruciform Building, University College London, Gower Street, London WC1E 6BT, UK; [þ] The Francis Crick Institute, 1 Midland Road, London NW1 1AT, UK; [#] South African Medical Research Council, Drug Discovery and Development Research Unit, Department of

Chemistry and Institute of Infectious Disease and Molecular Medicine, University of Cape Town, Rondebosch 7701, South Africa.

Supporting information

ABSTRACT: A lead-optimization programme around a 2,6-imidazopyridine scaffold was initiated based on the two early lead compounds, **1** and **2**, that were shown to be efficacious in an in vivo humanized *Plasmodium falciparum* NODscidIL2Rγnull (*P.f.*NSG) mouse malaria infection model. The observation of atypical dose-response curves when some compounds were tested against multi-drug resistant malaria parasite strains guided the optimization process in order to define a chemical space that led to typical sigmoidal dose-response and complete kill of multi-drug resistant parasites. After a structure and property analysis identified such a chemical space, compounds were prepared that displayed suitable activity, ADME, and safety profiles relative to cytotoxicity and hERG inhibition.

KEYWORDS: antiplasmodial activity, atypical dose-response curves, chemical space, permeability, pharmacokinetics.

Introduction: The strategic plan towards malaria disease control and elimination that was approved by the World Health Organization (WHO) in 2015 set ambitious objectives for 2030.[1] These included the reduction of malaria incidence and mortality rates by 90%, the elimination of the disease in 35 countries, and the preclusion of malaria resurgence in all countries that had been declared malaria-free. Although these goals seemed achievable in view of the progress that had been made over the past decades, the most recent reports

by the WHO and Wellcome Trust revealed worrying trends with regards to disease recrudescence and resistance development, thus compromising the likelihood of achieving the projected objectives.[2,3] In this context, there is an urgency for the malaria scientific community to join forces and ideas in order to rapidly identify and develop new chemical entities for the treatment and prevention of both drug sensitive and resistant malaria.

Furthering the work that has recently been reported on a 2,6-imidazopyridine series of antimalarial compounds that brought about two early lead compounds, **1** and **2** (Figure 1),[4] a lead optimization programme was conducted in order to identify potential compounds meeting late lead criteria as defined by the Medicines for Malaria Venture (MMV).[5] In particular, we focussed on improving pharmacokinetic (PK) parameters to reduce clearance and thus increase half-life and bioavailability, as well as on enhancing safety margins over cytotoxicity and human Ether-a-go-go-Related Gene (hERG) inhibition. Herein we discuss the optimization studies that were undertaken in order to advance to a late lead, along with the unexpected obstacles that required mitigation in the process.

Figure 1. Structure of compounds **1** and **2**

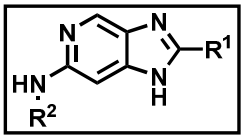

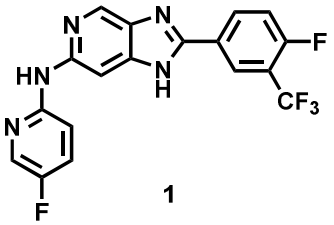

1

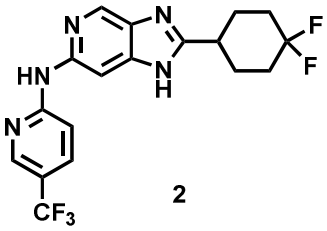

2

Results and discussion:

Chemistry: Compounds were prepared according to a previously described general synthetic route from commercially available 2,4-dichloro-5-nitropyridine **3**.[4] From intermediate **4**, two different routes were followed depending on the nature of the $\mathbf{R^2}$ 2-pyridine substitution.

For compounds **6-29** (Scheme 1 – Route A), the 2-aminopyridine to be incorporated at the 6-position ($\mathbf{R^2}$) of the imidazopyridine scaffold was prepared from 5-fluoro-2-nitropyridine by fluorine displacement with the corresponding saturated cyclic amine (e.g., piperazine, morpholine, piperidine), followed by reduction of the nitro functionality to the desired amine (80-90% over two steps). Subsequent Buchwald-Hartwig coupling with the imidazopyridine intermediate **4** using previously described conditions[4] afforded intermediates **5**. In a final step, the *para*-methoxybenzyl (PMB) and, in some cases, the *tert*-butoxycarbonyl (Boc) protecting groups, were removed using neat trifluoroacetic acid (TFA) to afford the desired 2,6-disubstituted imidazopyridines **6-29**.

For the amides **33-55**, and **62-71**(Scheme 1 – Route B), the methyl ester derivatives **30** were prepared from intermediate **4** and the corresponding methyl esters of the 4- or 5-(2-amino)pyridine carboxylic acids under Buchwald-Hartwig conditions as previously described.[4] After removing the PMB-protecting group, the pyridine carboxylic acids **32** were obtained in 53-95% yield from lithium hydroxide hydrolysis. Subsequently, coupling with the appropriate amine under standard amide coupling conditions afforded the desired amides in 23-49% yield. For compounds containing an NBoc group, an additional step was required, wherein the Boc-protecting group was removed in neat TFA.

When the alkylated piperazines were not commercially available, these were prepared via reductive amination with the appropriate aldehydes or ketones, and sodium triacetoxyborohydride, or via nucleophilic substitution on the corresponding alkyl bromide in the presence of potassium carbonate.

The preparation of compounds **56-61** has been described previously.[4]

Scheme 1. Synthetic route leading to the preparation of compounds **6-29**, **33-55**, and **62-71**.

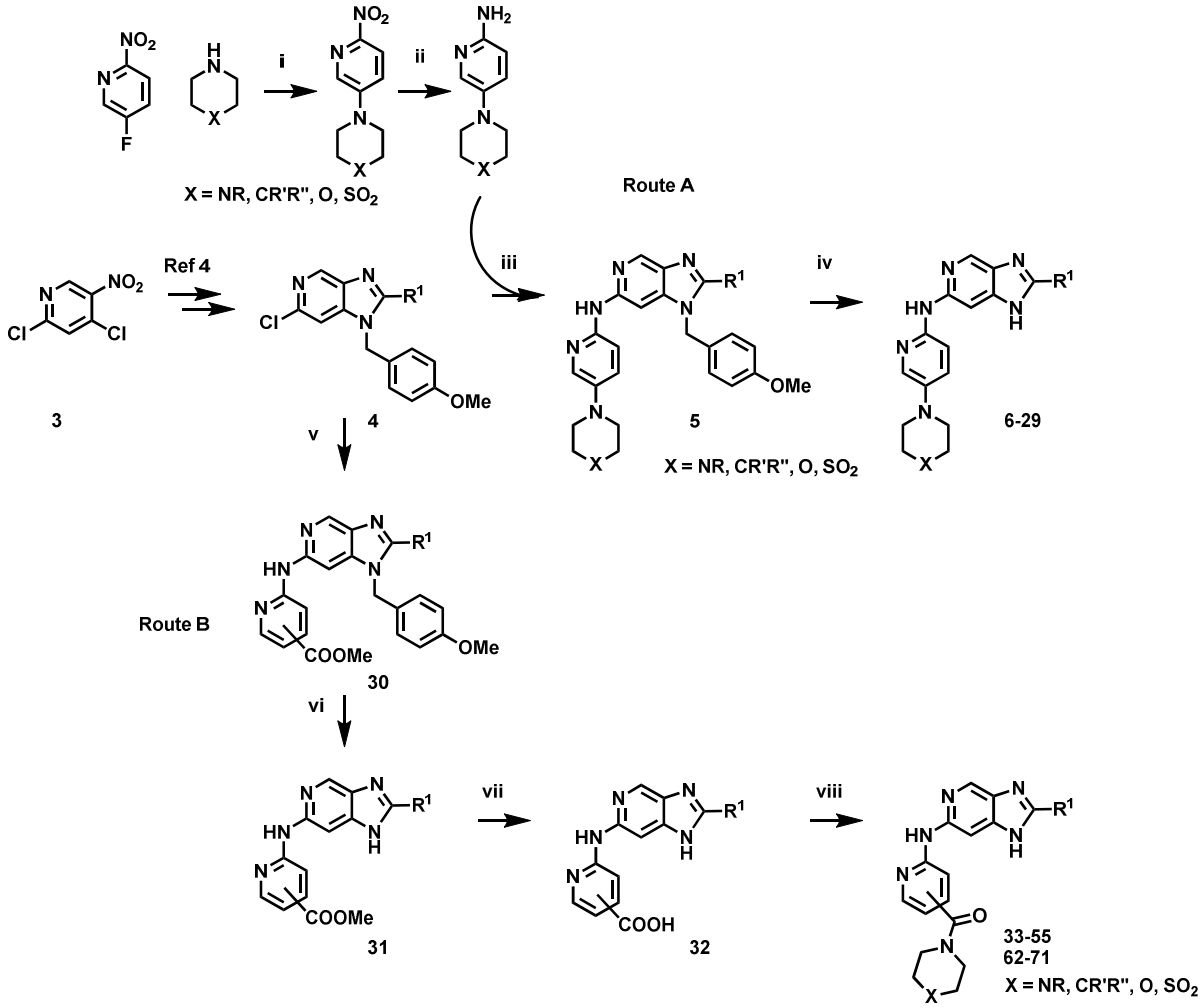

Reagents and conditions: Route A – (i) DIPEA (1.1 equiv), EtOH, 80°C , 80-95%; (ii) H_2, AcOH, Pd-C, 95-100%; (iii) NH_2R^2 (1.2 equiv), $Pd_2(dba)_3$ (0.04 equiv), BrettPhos (0.06 equiv), Cs_2CO_3 (1.4equiv), *tert*-BuOH/Toluene (1:1), 110°C, 16h, 20-80%; (iv) TFA, 100°C, 12h, 10-99%; Route B – (v) NH_2-C_6H_4-COOMe (1.2 equiv), $Pd_2(dba)_3$ (0.04 equiv), BrettPhos (0.06 equiv), Cs_2CO_3 (1.4 equiv), *tert*-BuOH/Toluene (1:1), 110°C, 16h, 90%; (vi) TFA, 100°C, 12h, 95%; (vii) LiOH.H_2O (5 equiv), dioxane/water(1:1) (0.25 M), 50°C, 12h, 53-95%; (viii) (a) Amine (1.2 equiv), HATU

(1.2 equiv), Et_3N (2.4 eq), DMF, 50°C, 12h, 23-49%; (b) if X = NBoc: TFA, 100°C, 12h, 20-95%.

Antiplasmodial activity, ADME (Absorption Distribution Metabolism and Excretion) profiling, and cardio- and cytotoxicity: All compounds were evaluated for in vitro antiplasmodial activity against the NF54 drug sensitive strain of *P. falciparum*. Selected compounds with NF54 IC_{50} < 1μM were tested against the K1 multi-drug resistant strain of *P. falciparum* to assess the potential for cross-resistance. In this work, a compound is considered to have potential for cross-resistance when (K1 IC_{50})/(NF54 IC_{50}) ≥ 4. Chloroquine and artesunate were used as reference compounds in all experiments.

To assess metabolic stability, selected compounds were subjected to a microsomal turnover assay in vitro with human, rat, and mouse liver microsomal preparations. The assay determines the percentage of compound remaining after a 30-minute incubation period in the presence of the microsomes.

Aqueous solubility was measured at pH 6.5 for compounds displaying NF54 IC_{50} < 500 nM.

Compounds with NF54 IC_{50} < 500 nM were also tested for cytotoxicity against Chinese Hamster Ovary (CHO) cells.

The activity against the hERG potassium channel was determined using in vitro IonWorks patch-clamp electrophysiology.[6]

All the methods used for the aforementioned assays are described in detail in the Supporting Information (sections B, C, D, E, and G, in that order).

Initial Optimization and atypical dose-response curves: Recently reported structure-activity-relationships (SAR) studies around the 2,6-imidazopyridine series led to the identification of two early lead compounds, **1** and **2** (Figure 1).[4] Good asexual blood stage (ABS) antiplasmodial activities (NF54 IC_{50} = 18 and 63 nM, respectively) were achieved, as well as good in vitro ADME properties (e.g., water solubility and metabolic stability). Moreover, when tested in vivo in a *P.f.*NSG mouse model of malaria, compounds **1** and **2** demonstrated good efficacy following a 4-time dosing regimen (ED_{90} = 4.2 and 5.6 mg/kg, respectively) and notably fast-killing kinetics. In order to advance towards a late lead, the main focus was on improving antiplasmodial activity (IC_{50} against a panel of *P.f.*strains < 10 nM) together with drug metabolism and pharmacokinetic (DMPK) parameters in order to achieve higher exposure and better in vivo efficacy, as well as on increasing safety margins over cytotoxicity and hERG inhibition (SI > 1000).

Further compound optimization from **1** and **2** involved continued alterations of the $\mathbf{R^1}$ and $\mathbf{R^2}$ substituents (Figure 1) in order to determine a favorable combination of potency and physicochemical properties that would translate to improved efficacy in the in vivo model. However, the initial plans for synthesis were put on hold, as a number of compounds displayed an unexpected abnormal dose-response curve when tested against the multi-drug resistant K1 parasite strain, a phenomenon that was not seen with sensitive strains, e.g., NF54, D6, or 3D7, at similar concentrations. Instead of showing the characteristic sigmoidal shape of a typical dose-response curve (Figure 2 – A), these compounds led to a biphasic curve, also referred to as bimodal in the literature,

displaying an increased survival profile at higher drug concentrations (Figure 2 – B). Such dose-response curves showing a similar effect, known as the Eagle effect, have also been observed with antibacterial drugs.[7] In addition to these biphasic curves, some compounds did not achieve complete parasite kill even at high concentrations (Figure 2 – C), which, besides preventing accurate IC_{50} determination, raised major concerns with regards to resistance potential. It is worth noting that these phenomena were also observed across various other resistant *P. falciparum* strains, including Dd2, HB3, 7G8, TM90C2B, V1/S, FCB. Assay repeats and inter-laboratory cross-validation experiments were performed and consistently resulted in atypical dose-response curves when the phenomenon occurred.

Figure 2. Shape of different dose-response curves with: **A)** a typical sigmoidal profile; **B)** a biphasic profile; **C)** incomplete parasite kill

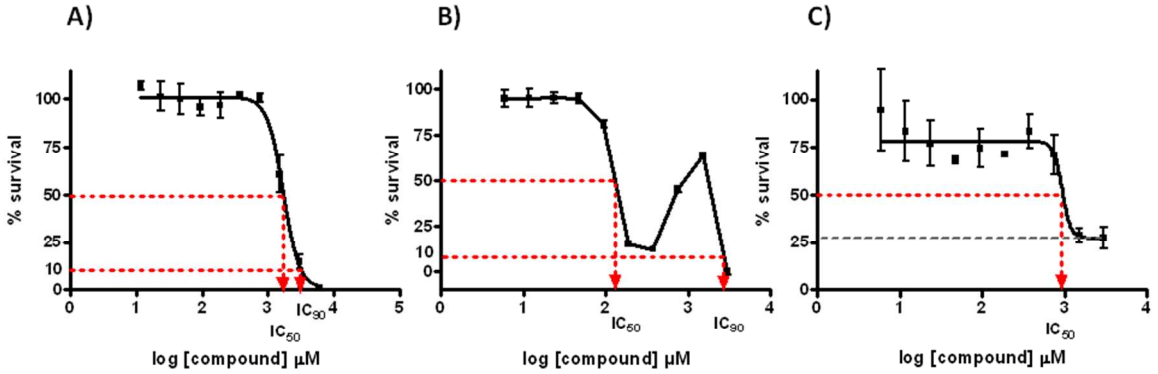

Whilst the IC_{50} was only marginally affected in resistant strains, since the 50% inhibition of parasite growth remained largely unchanged relative to sensitive strains, the inhibitor concentration required to reach below the limit of detection of parasitemia was highly

affected for compounds displaying atypical dose-response curves, thus significantly increasing the IC_{90} value in comparison with a standard sigmoidal curve, as exemplified by compounds **56-61** in Table 1. The much greater shift in activities between sensitive and resistant strains observed for IC_{90} values compared with IC_{50}'s can be interpreted as a typical sign of cross-resistance (K1 IC_{90}/NF54IC_{90} $\geq$ 4), as indicated in literature examples reporting similar dose-response curves in resistant field isolates, or following resistant selection experiments.[8, 9, 10, 11] Biphasic dose-response curves may also be observed in the presence of mixed parasite populations, and/or drugs with two different mechanisms of actions.[12, 13]

Table 1. Comparison of IC_{50}'s and IC_{90}'s in NF54 and K1 *P.falciparum* strains for exemplary compounds with atypical dose-response curves

Compound	Structure	IC_{50} (nM)[a,b]			IC_{90} (nM)[a,b]		
		NF54	K1	K1/NF54	NF54	K1	K1/NF54
56	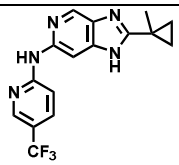	**48**	**90**	**1.9**	**72**	**846**	**12**
57	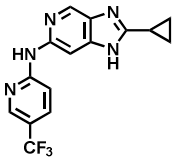	**78**	**147**	**1.9**	**125**	**758**	**6.1**
58	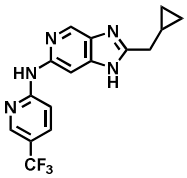	**63**	**114**	**1.8**	**87**	**1473**	**17**

59	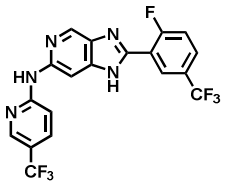	**45**	**118**	**2.6**	**79**	**1638**	**21**
60	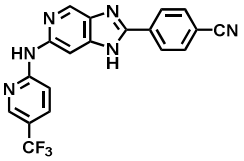	**23**	**61**	**2.7**	**39**	**1123**	**29**
61	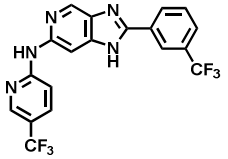	**50**	**118**	**2.4**	**80**	**1302**	**16**

[a] Mean from n values of ≥2 independent experiments with multidrug resistant (K1) and sensitive (NF54) strains of *P. falciparum* using the [^{3}H]-hypoxanthine incorporation assay.[14] The majority of the individual values varied less than 2x (maximum 3x).

[b] Chloroquine and artesunate were used as reference drugs in all experiments. Against NF54 and K1, our laboratory standard IC_{50} values for chloroquine and artesunate are 16/194 nM and 4.0/3.0 nM, respectively (mean from ≥10 independent assays). IC_{50} values that differed more than 3x from laboratory standard values were not included in the analysis.

Owing to the observed cross-resistance at the IC_{90} level with multi-drug resistant strains, efforts proceeded towards the identification of a chemical space that would not show an upswing in parasitemia at higher concentrations, before resuming lead optimization.

Identification of a suitable chemical space: An initial analysis of structural features that might be responsible for the undesired dose-response curves observed with the K1 multidrug-resistant strain did not immediately suggest any obvious trend. Therefore, in order to investigate if a chemical space that allowed for normal dose-response curves was

identifiable, the existing data was analyzed using computational tools such as StarDrop.[15] Possible correlations between various physicochemical properties, and the shape of the dose-response curve were examined. For each property [e.g., solubility, logD, molecular weight (MW), topological polar surface area (TPSA)], we looked at the distribution of compounds that resulted in normal or atypical dose-response curves in relation to increasing values of the described property (Figure 3). No correlations were identified with regards to molecular weight, solubility, or lipophilicity, as compounds with atypical curves were found across the whole range of each. However, the TPSA (Figure 3D) did offer a potential correlation, albeit unexplained. Compounds having a lower calculated TPSA between 65 and 70 $Å^2$ were more likely to display an atypical dose-response curve than compounds with a higher TPSA. Derivatives containing a nitrile also triggered an atypical dose-response curve.

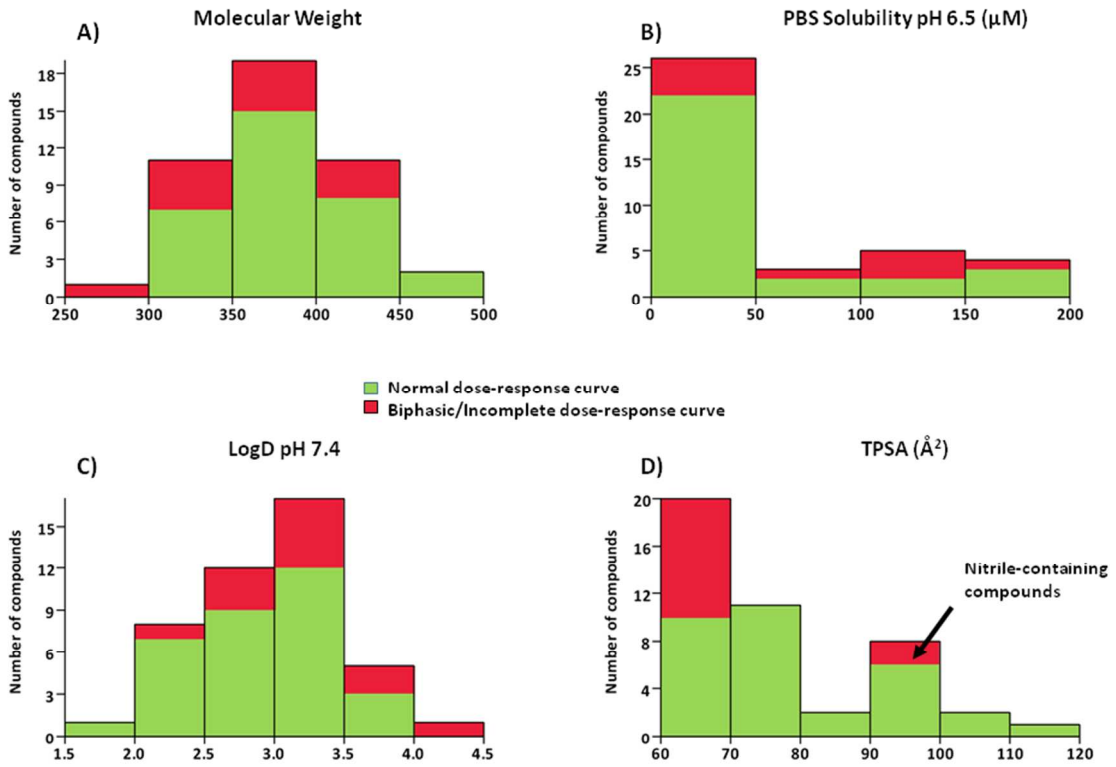

Figure 3. Examining potential correlations between physicochemical parameters and the shape of the K1 dose-response curve.

Subsequent substituent-based analysis (Figure 4) suggested that amide moieties or saturated heterocycles such as morpholine, piperidine, or piperazine on the $\mathbf{R^2}$ pyridine allowed a move away from the atypical curve phenomenon, whilst retaining favorable in vitro ADME properties (e.g., solubility and metabolic stability) as determined previously.[4] On the other hand, small electron withdrawing groups such as fluorine, trifluoromethyl, or nitrile on the $\mathbf{R^2}$ pyridine gave more erratic results depending on the nature of the $\mathbf{R^1}$ substituent. The latter findings correlate well with the former

observations related to TPSA and the tendency for nitrile-containing derivatives to result in atypical dose-response curves.

With regards to the **R**[1] position, it was more difficult to identify trends, since both aromatic and saturated systems could lead to an atypical curve. Overall, the exploration of a chemical space containing amide groups and/or saturated heterocycles on the aminopyridine at **R**[2] seemed to be the best compromise to continue our lead optimization programme, as it had previously been established that a combination of aromatic substituents at both **R**[1] and **R**[2] was detrimental for aqueous solubility and cytotoxicity margins.[4]

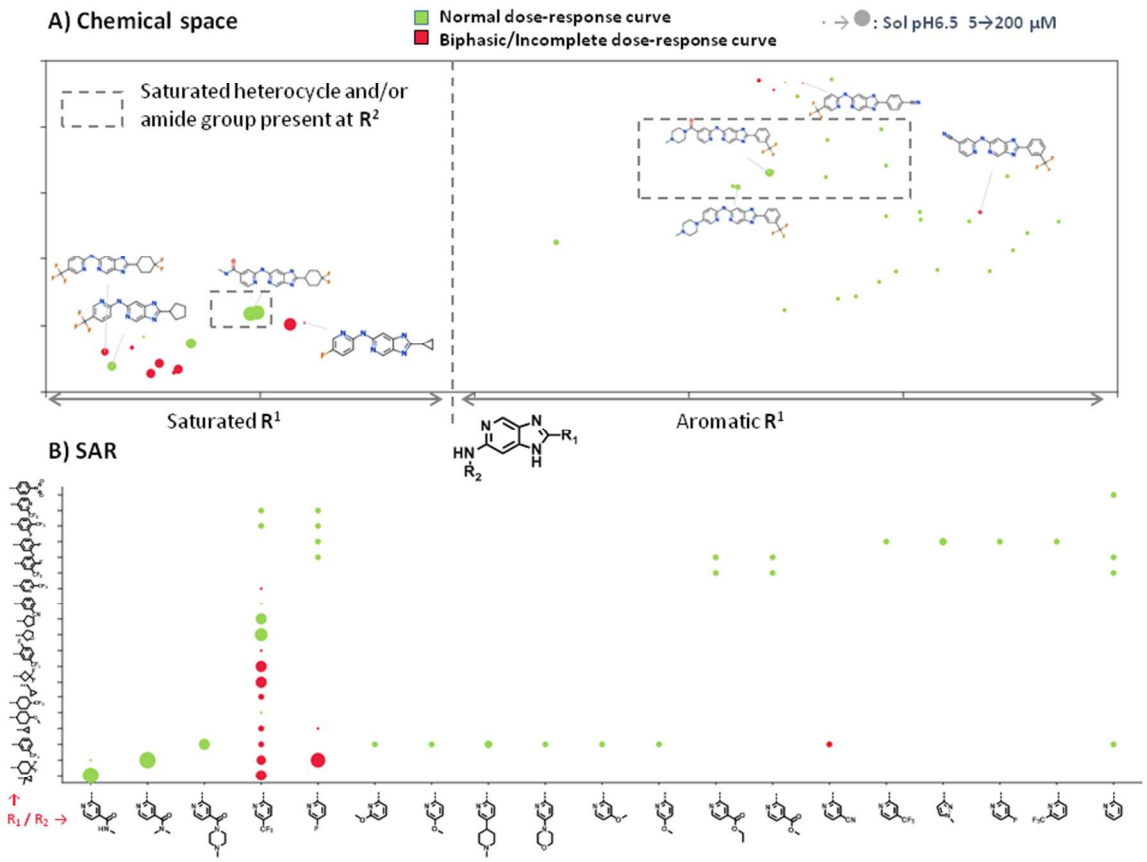

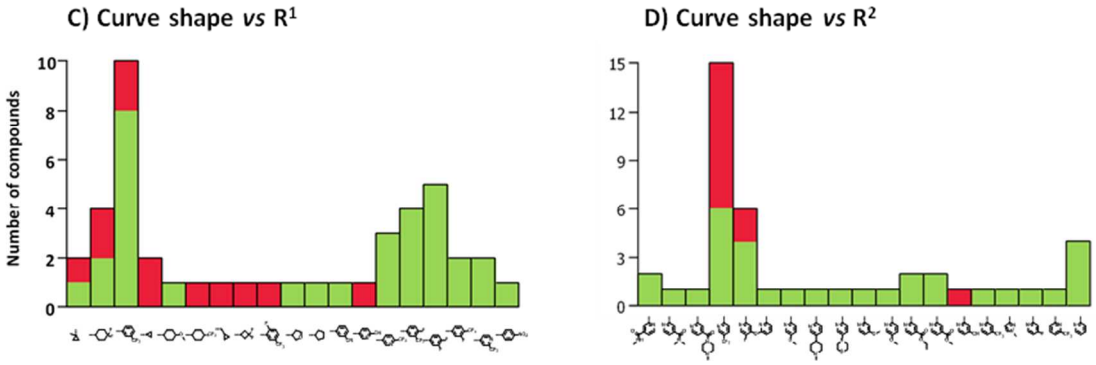

Figure 4. Substituent-based analysis to identify features leading to atypical dose-response curves in the multidrug resistant K1 strain **A)** Analysis of the chemical space; **B)** SAR analysis; **C)** Curve shape *vs* $\mathbf{R^1}$; **D)** Curve shape *vs* $\mathbf{R^2}$.

Validation of the identified chemical space and compound optimization: Based on the aforementioned observations, a variety of compounds were designed and prepared in order to explore diverse carboxamide groups and/or saturated heterocycles at $\mathbf{R^2}$ combined with favored $\mathbf{R^1}$ substituents, with the anticipation that they would retain high antiplasmodial activity and suitable ADME properties (Table 2). Within this context, $\mathbf{R^1}$ was either a substituted phenyl or saturated ring, and $\mathbf{R^2}$ was a 2-pyridylcarboxamide or a 2-pyridine bearing a saturated heterocyclic ring at the 4-position, making four subsets of compounds A, B, C, and D as shown on Figure 5. Gratifyingly, the new compounds all displayed a normal dose-response curve against the multi-drug resistant K1 parasite strain, thus supporting our analyses and confirming that the selected chemical space was suitable for further optimization of attributes towards identifying a late lead.

Figure 5. Preferred compound subsets for further SAR exploration

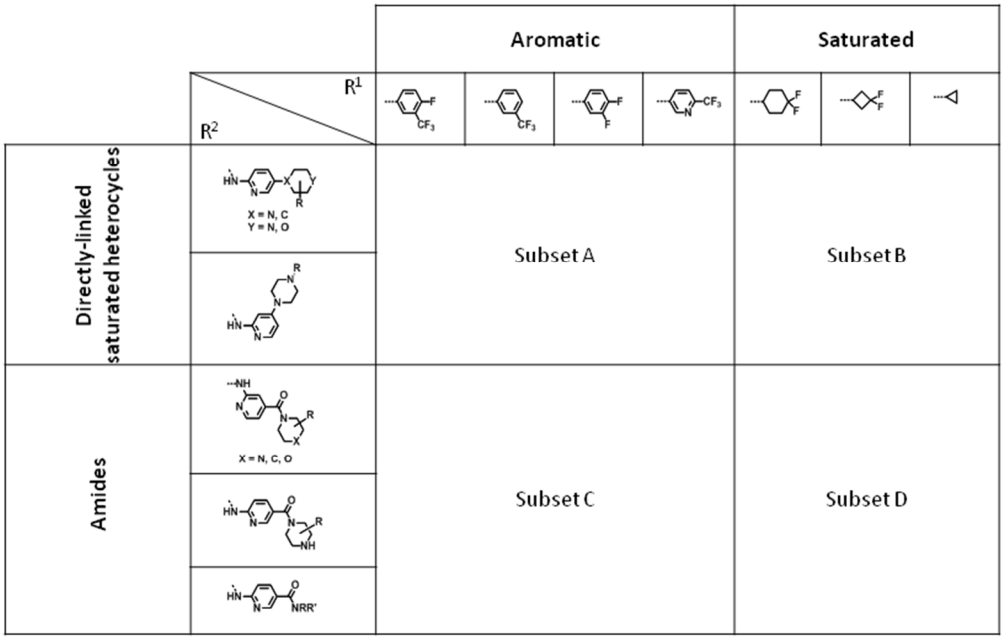

Aromatic $\mathbf{R^1}$ substituents generally led to better in vitro activity against both NF54 and K1 *P. falciparum* strains than saturated groups. A clear SAR trend for $\mathbf{R^1}$ was identified within the amide subset C, with 3-CF_3, 4-F substitutions giving better potency than 3-CF_3, 3,5-diF and 4-F, 3-pyridine substitutions, in this order. In contrast, for any given directly-linked saturated heterocycle on the $\mathbf{R^2}$ pyridine from subset A, activities were more homogeneous across the different $\mathbf{R^1}$ variations.

With respect to saturated $\mathbf{R^1}$ groups (subsets B and D), the 4,4-difluorocyclohexyl ring gave the highest ABS activities. However, the combination of saturated groups at both $\mathbf{R^1}$ and $\mathbf{R^2}$ seemed disadvantageous for potency, with the exception of compounds **27** and **25** that displayed IC_{50}'s below 50 nM against NF54 and/or K1 parasite strains.

Overall, derivatives with directly-linked piperazine substitutions on the $\mathbf{R^2}$ pyridine (subset A) were highly potent, but seemed more disposed to cytotoxicity than their amide analogues, as exemplified by the matched pairs **13**/**38** (SI = 75/468), **20**/**44** (SI = 135/>500), and **11**/**36** (SI = 100/882). $\mathbf{R^2}$ pyridine carboxamides bearing a polar group significantly lost activity, as shown with **37**, **41**, and **42** (NF54 IC_{50}'s ranging from 360 to 1200 nM).

Aqueous solubility was variable across subsets A, B, and C, depending on the nature of the piperazine substitution on the $\mathbf{R^2}$ pyridine. When the piperazine distal nitrogen was alkylated, aqueous solubility tended to decrease, although the *tert*-butyl analogue **39** retained high water solubility (200 μM at pH 6.5). Likewise, replacement of the piperazine with a morpholine (**11**, **17**, **36**, **45**, and **49**) or a piperidine, as in **46** or **51**, lowered aqueous solubility at pH 6.5 to less than 5 μM, preventing these compounds from progressing to further assays. On the other hand, incorporation of methyl groups on the adjacent carbons of the distal piperazine nitrogen increased solubility to ≥ 165 μM (e.g., **16**, **20**, **34**, **35**, **40**, **44**, and **48**).

With respect to metabolic stability, trends seemed to be conserved across the two subsets A and C, with the substitution pattern of the piperazine appended to $\mathbf{R^2}$ playing a major role in the compound propensity to be metabolized. Metabolic instability as in **38** was attributed to N-dealkylation and oxidation on the piperazine moiety as indicated by a metabolite identification study (Supporting Information – Section F-1). This was addressed by methylation of one or two of the carbons adjacent to the piperazine nitrogen, resulting in more stable compounds (e.g., **34**, **35**, and **40**). The morpholine

derivatives were moderately to highly susceptible to metabolism as shown by **11**, **17**, and **36**.

Table 2. Antiplasmodial activity, solubility, metabolic stability and cytotoxicity data for compounds **6 – 29** and **33 – 55**.

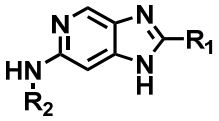

Subset	Compound #	R^1	R^2	NF54/K1 IC_{50} (nM)[a,b]	Solubility pH 6.5 (µM)	% remaining at 30 min (h,r,m)	CC_{50} CHO (µM) (SI)
A	**6**	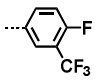	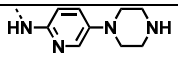	200/540	180	92/59/55	14 (70x)
	7		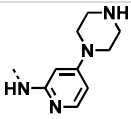	420/330	95	98/73/78	31 (74x)
	8		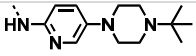	20/-			
	9		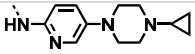	82/550	5		23 (280x)
	10		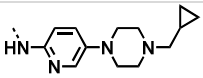	39/82	75	52/36/41	41 (1000x)
	11		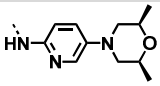	84/310	<5	17/19/6	8.5 (100x)
	12	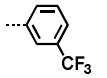	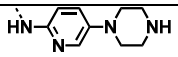	150/190	200	200/97/97	4.6 (30x)
	13		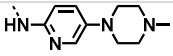	69/66	66	68/46/35	5.2 (75x)
	14		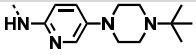	11/12	50		99 (5000x)

	15			14/72	130		1.7 (121x)
	16			25/200	180	71/53/63	25 (1000x)
	17			39/77	<5	11/74/54	4.2 (110x)
	18			170/450	<5	92/73/75	33 (194x)
	19			36/74	10	7/9/14	1.2 (33x)
	20			20/164	175	63/66/76	2.7 (135x)
	21			280/-	190	98/97/87	50 (178x)
	22			700/-	40		
	23			10/100	10	93/55/68	1.2 (30x)
B	**24**			1600/-			
	25			28/91			
	26			630/-			
	27			39/21	10	59/64/61	4.5 (115x)
	28			260/1000	190	86/52/54	50 (200x)
	29			270/-			
C	**33**			55/190	<5	77/53/93	30 (545x)

	34		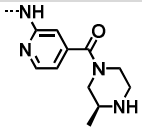	87/340	165	77/53/93	> 50 (> 575x)
	35		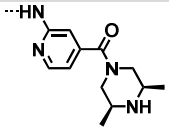	26/100	200	89/90/90	29 (1115x)
	36		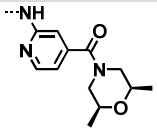	34/85	<5	63/65/41	30 (882x)
	37		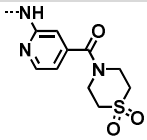	1200/1500			
	38		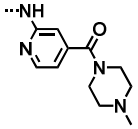	94/157	120	68/48/26	44 (468x)
	39		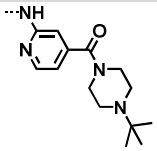	20/61	200	65/48/26	42 (2100x)
	40		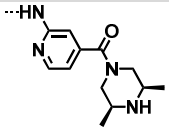	35/140	200	86/87/86	37 (1057x)
	41		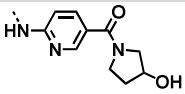	1000/-			
	42		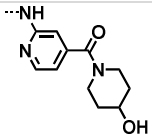	360/140			> 50 (>140x)
	43		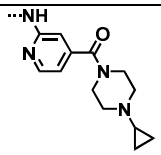	210/510	<5		>50 (> 238x)

	44		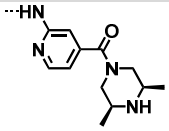	96/460	100		>50 (> 500x)
	45		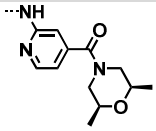	115/250	<5		>50 (> 450x)
	46		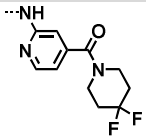	21/170	<5	95/68/77	29 (1380x)
	47		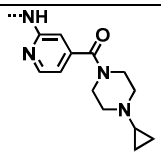	438/479			>50 (> 1000x)
	48		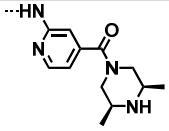	520/1300	200		
	49	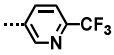	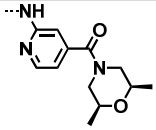	170/420	<5		>50 (> 300x)
	50		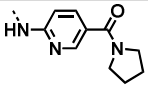	350/-	<5	93/83/85	220 (630x)
	51		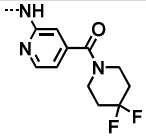	97/130	<5		1 (10x)
	52		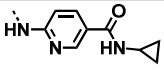	480/-	<5	84/89/87	228 (475x)
D	**53**		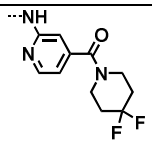	480/-			> 50 (> 100x)

	54		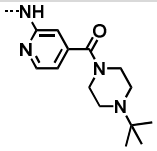	4500/2800			
	55		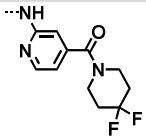	1200/1100			> 50 (> 400x)

[a] Mean from n values of ≥2 independent experiments with multidrug resistant (K1) and sensitive (NF54) strains of *P. falciparum* using the parasite lactate dehydrogenase (pLDH) assay.[16, 17] The majority of the individual values varied less than 2x (maximum 3x). The values were confirmed in the [^{3}H]-hypoxanthine incorporation assay.[14]

[b] Chloroquine and artesunate were used as reference drugs in all experiments. Against NF54 and K1, our laboratory standard IC_{50} values for chloroquine and artesunate are 16/194 nM and 4.0/3.0 nM, respectively (mean from ≥10 independent assays). IC_{50} values that differed more than 3x from laboratory standard values were not included in the analysis.

Aliphatic amides, in particular substituted ethylamides, were also evaluated to investigate the impact of more flexible and longer side chains on ABS activity. However, these analogues were only moderately to poorly active and, therefore, were not profiled further (Compounds **S1-S6**, Supporting Information – Section A, Table A-2).

A number of preferred compounds with favorable activity and ADME profiles, including **12**, and **35**, were identified from this SAR exploration, and selected for further in vivo studies, starting with mouse pharmacokinetic experiments in order to identify potential PK-related liabilities.

Assessment of activity against the hERG channel: Selected compounds were evaluated for hERG activity with the goal of identifying compounds with inhibitory activity (IC_{50}) greater than 10 μM in order to minimize cardiotoxicity risks. The results are summarized in section G of the Supporting Information.

Trends relating hERG activity to structural features were difficult to assess since the dataset was small. Nonetheless, morpholine derivatives tended to be more active against the hERG potassium channel compared with their piperazine analogues (e.g., **17**/**12** hERG IC_{50} = 0.5 / 30 μM / **36/35** hERG IC_{50} = 5.3 / 13 μM). Piperazine moieties somewhat appeared beneficial with respect to decreasing hERG activity, and indeed all the compounds that met the criteria with regards to cardiac safety risks bore a piperazine group at $\mathbf{R^2}$, including **12**, **19**, **33**, **35**, and **38**.

In vivo pharmacokinetics studies: Selected compounds, with suitable aqueous solubility and safety margins over cytotoxicity, were dosed in mice in order to evaluate drug exposure and pharmacokinetics parameters (Table 3). Although **12** only exhibited moderate ABS activity (NF54 IC_{50} = 150 nM), a PK study was of interest as it showed high solubility and low in vitro intrinsic clearance. Following intravenous (i.v.) administration, clearance was moderate (29 mL/min/kg). Compound **12** was highly distributed into tissues (Volume of distribution, Vd = 22 L/kg), resulting in a long plasma half-life. However, its oral bioavailability was very low (2%), which was attributed to poor permeability. Metabolism of the parent compound was minor according to the metabolite identification study, mainly resulting in oxidation of the piperazine ring (Supporting Information – Section F-2).

To evaluate the impact of increased lipophilicity on the piperazine moiety, resulting from the addition of two adjacent methyl groups or a *tert*-butyl group on the piperazine nitrogen, PK studies were performed with **35** and **39**, respectively (logD = 2.5 and 2.9 respectively, compared to 2.3 for **12**). Both compounds behaved similarly and were cleared rapidly when dosed intravenously with a significant distribution into tissues (CL = 99 mL/min/kg, Vd = 58 L/kg for **35**, and CL = 68 mL/min/kg, Vd = 117 L/kg for **39**), resulting in a long plasma half-life (7h and 19h, respectively). Again, when dosed orally, **35** and **39** were not absorbed (BA = 1% and 2 %, respectively), indicating that the low lipophilicity of **12** was not the main contributor to poor absorption, and that other parameters needed to be taken into account to improve bioavailability (e.g., number of hydrogen-bond donors (HBD), pKa, size, efflux). A metabolite identification study on the **35** in vivo i.v. PK blood samples, identified only minor metabolites. (Supporting Information – Section F-3).

In this light, the morpholine and the difluoropiperidine analogues of **35**, **36** and **46**, respectively, were evaluated in vivo to investigate the impact of the piperazine distal nitrogen on absorption. In both cases, bioavailability remained very poor. For **36**, clearance and volume of distribution were significantly reduced (14 mL/min/kg compared to 99 mL/min/kg, and 4.8 L/kg compared to 58 L/kg, respectively) but did not contribute to enhancing bioavailability. No improvement in any of the PK parameters was observed with **46**.

Table 3. PK parameters for compounds **12**, **35**, **36**, **39**, and **46**.

Compound #	Method	Dose (mg/kg)	$t_{1/2}$ (h)	Blood Cl (mL/min/kg)	Vd (L/kg)	C_{max} (µM)	T_{max} (h)	$AUC_{0-\infty}$ (min.µM)	F (%)
12	p.o.	20	—	—	—	0.02	0.5	35	2
	i.v.	2	9	29	22	2.0	—	174	—
35	p.o.	20	—	—	—	0.005	0.5	3	1
	i.v.	2	7	99	58	0.6	—	40	—
36	p.o.	20	—	—	—	0.16	1	21	1
	i.v	2	4	14	4.8	4.8	—	271	—
39	p.o.	20	—	—	—	0.04	0.5	12	2
	i.v	2	19	68	117	—	—	56	—
46	p.o.	20	—	—	—	0.60	1	68	6
	i.v.	2	4	35	13	1.5	—	115	—

Permeability and efflux-ratio: From the PK studies, it seemed apparent that permeability and/or efflux were the main limiting factors to absorption. This posit was further confirmed for **35** by conducting permeability assays with Caco-2 cells in the presence and absence of the P-gp inhibitor verapamil. In the presence of verapamil, the efflux ratio of **35** was reduced by more than 50%, from 29.4 to 12.9. However, the fact that the efflux ratio remained high even in the presence of verapamil suggested that other transporters than P-gp could also be involved. To mitigate efflux, structural modifications were considered to decrease the TPSA to less than 90Å^2, lower the number of HBD to two or less, and maximize the lipophilicity ligand efficiency (LLE)[18,19] (LLE > 5) as suggested by Hitchcock.[20] Although it is further suggested to reduce TPSA down to

below 70 Å^2, the TPSA was kept between 70 Å^2 and 90 Å^2 due to the indication that TPSA values <70 Å^2 were more likely to bring about atypical dose-response curves. Moreover, we hypothesized that reducing the basicity of the compound would increase permeability by allowing our molecules to be in a single-charged form at the pH (6.5) of the gastrointestinal tract.

In line with these considerations, bridged amines were introduced to reduce TPSA and potentially the basicity of the compounds, as exemplified by **64**, **65**, **66**, **67**, and **68** (Table 4). A pKaH < 7.5 would allow a nitrogen atom to be non protonated at pH = 6.5 associated with the intestinal tract. Furthermore, alkylation of the distal nitrogen was designed to bring down the number of HBD to two (i.e., for **62**, **63**, **65**, **67**, **68**, **70**), and to increase potency by adding lipophilicity (Table 4). However, no improvements in permeability and efflux were observed with these changes, as shown by the values from the Caco-2 assay. In addition, although cLogP values of all compounds remained in a desirable 2-to-4 range, their LLE values were lower than that of the reference compound **35** (LLE = 4.8) due to lower NF54 activity.

Slight structural changes in the scaffold or substitution pattern as in **71**, and **69** were also investigated to evaluate the impact on efflux, since it has previously been demonstrated that minor alterations to the structure could significantly influence efflux.[21] However, these modifications proved not to be beneficial.

As the efforts to address poor permeability and high efflux were in vain, high efflux ratios may be inherent to the compound structure as precedents for amide functionality leading to high efflux ratios have previously been reported.[22]

The conundrum thus presents itself: in order to move away from abnormal dose-response against K1 resistant parasites, the allowed chemical space for lead optimization was limited. Compound permeability became more problematic and the defined chemical space too narrow to achieve both good antimalarial activity and pharmacokinetic properties.

Table 4. Predicted physico-chemical properties and activity, solubility and permeability data of compounds **62-71**.

Scaffold	R^1	Compounds	R^2	TPSA HBD cLogP [a]	Predicted pKaH (R^2 distal N) (Chemicalize/ Percepta) [b]	IC_{50} NF54/K1(nM)[c,d] Solubility pH6.5 (µM) Caco2 A>B (P_{app}x10^{-6} cm/s)/ efflux ratio	LLE [d]
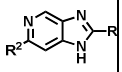		**62**	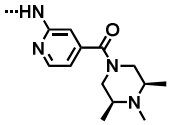	84.7 2 3.3	7.4/7.5	20/11 180 1.7/12	4.4
		63	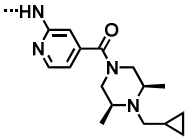	84.7 2 4.0	8.1/7.9	280/440 200 0.14/9.2	2.3
		64	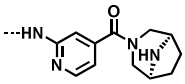	93.5 3	9.6/8.2	250/570 180	4.0

				2.6		-		
		65	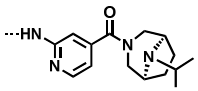	84.7 2 3.8	8.2/8.2	67/150 195 0.66/83	3.4	
		66	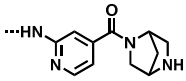	93.5 3 2.3	9.5/8.1	1200/1200 115 -	3.6	
		67	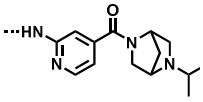	84.7 2 3.5	7.9/9.7	120/230 155 -	3.4	
		68	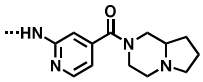	84.7 2 3.0	8.5/9.0	35/84 85 -	4.4	
		69	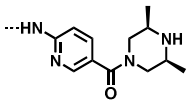	93.5 3 2.8	8.0/8.3	92/400 50 No permeation/83	4.3	
		**70**	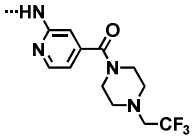	84.7 2 3.1	0.9/3.7	80/- < 5 5.3/4.9	4.0	

				93.5		70/148		
		71		3	8.0/8.3	185	4.2	
				2.8		0.65/68		

[a] cLogP calculated with Stardrop

[b] Chemicalize and Percepta from ACDLabs were used to predict pKaH values of the distal piperazine nitrogen. A 0.5-log unit difference between the two predicted values was generally observed, except for compounds **64**, **66**, **67**, and **70** where the difference was much bigger, in which case it was difficult to get an estimate.

[c] Mean from n values of ≥2 independent experiments with multidrug resistant (K1) and sensitive (NF54) strains of *P. falciparum* using the pLDH assay.[16, 17] The majority of the individual values varied less than 2x (maximum 3x).

The majority of the individual values varied less than 2x (maximum 3x)

[d] Chloroquine and artesunate were used as reference drugs in all experiments. Against NF54 and K1, our laboratory standard IC_{50} values for chloroquine and artesunate are 16 nM / 194 nM and 4.0 nM / 3.0 nM respectively(mean from ≥10 independent assays). IC_{50} values that differed more than 3x from laboratory standard values were not included in the analysis.

[d] LLE = NF54 pIC_{50}-clogP

Conclusion:

Following the identification of two compounds meeting the early lead criteria as defined by MMV, we initiated a lead optimization programme towards identifying a late lead compound suitable for further development. An unexpected and undesired phenomenon leading to atypical dose-response curves against multi-drug resistant parasites was identified during the lead optimization campaign that needed to be resolved. Structure and property analysis identified a chemical space where the atypical dose-response

curves did not occur. Compounds were prepared that displayed suitable ABS activity, ADME and safety profiles, relative to cytotoxicity and hERG inhibition (e.g. **12**, **35**). However, the restricted chemical space led to compounds with poor pharmacokinetics, due to low permeability and high efflux. To continue lead optimization with this series, a differentiated chemical space needs to be identified, wherein the normal sigmoidal dose-response behavior against resistant malaria parasites is retained, whilst favorable in vivo pharmacokinetic properties are devised, in particular oral bioavailability.

Experimental section:

All commercially available chemicals were purchased from either Sigma-Aldrich or Combi-Blocks. Unless otherwise stated, all solvents used were anhydrous. ^{1}H NMR spectra were recorded on a Brucker Spectrometer at 300 or 400 MHz. ^{13}C NMR spectra were recorded at 75 or 100 MHz on a Brucker Spectrometer. Analytical thin-layer chromatography (TLC) was performed on aluminium-backed silica-gel 60 F_{254} (70-230 mesh) plates. Column chromatography was performed with a Teledyne ISCO CombiFlash® RF system using Silia*sep* universal flash cartridges from Silicycle (FLHR10030B). Chemical shifts (δ) are given in ppm downfield. Coupling constants, *J*, are recorded in Hertz (Hz). Purity was determined by LCMS, and all compounds were confirmed to have > 95% purity. The data that is not shown below is supplied in the Supporting Information (Section A).

General procedure for Buchwald coupling: Chloro intermediate **4** (1equiv) was dissolved in *tert*-butanol/ toluene (1:1) with the appropriate amine (1.5 equiv), BrettPhos

(0.06 equiv) and Cs_2CO_4 (1.4 equiv). The resulting mixture was flushed with nitrogen for 15 minutes, at which time $Pd_2(dba)_3$ was added. The solution was heated at 110°C for 12 hours. Water was then added and the solution was extracted with EtOAc. The combined organic layers were dried over Na_2SO_4 and concentrated under reduced pressure. The compound was purified on silica gel using a gradient of MeOH in DCM as eluting system.

General procedure for the preparation of carboxylic acids: Methyl ester (1 equiv) was dissolved in dioxane/water (3:1) (0.25 M) with $LiOH,H_2O$ (5 equiv) and the resulting mixture was stirred at 50°C for 12 h. The reaction was monitored by LC/MS. Once the reaction was complete, the solution was acidified to pH2 with a 2M HCl solution. The resulting mixture was extracted with EtOAc. The organic layer was washed with water and brine, dried over Na_2SO_4 and concentrated under reduced pressure. No further purification was required. The carboxylic acids were obtained in 70-90% yield.

General procedure for the preparation of amides from their corresponding carboxylic acid: The appropriate carboxylic acid (1equiv) was dissolved in DMF (0.1 M) with the appropriate amine (1.2 equiv), HATU (1.2 equiv) and Et_3N (2.4 equiv). The resulting mixture was stirred at 50°C for 12h, at which point water was added. The solution was extracted with EtOAc. The organic layer was washed with a 10% LiCl solution to get rid of the residual DMF, dried over Na_2SO_4 and concentrated under reduced pressure. Crystallization of the residue with EtOAc afforded the desired amides in 23-49% yield.

General procedure for PMB- and Boc-deprotection: Intermediates **5** or **30** were stirred in neat TFA at 100°C and the advancement of the reaction was monitored by LCMS. Once the reaction was completed, TFA was removed under reduced pressure and the residue was dissolved in DCM/MeOH (9:1) and stirred with Amberlyst A21 for 1h. The resin was filtered of and the filtrate concentrated under reduced pressure. The residue was purified by flash chromatography using DCM/MeOH (0.5M NH_3) as eluting system (100:0 to 85:15)

N-(5-(Piperazin-1-yl)pyridin-2-yl)-2-(3-(trifluoromethyl)phenyl)-1H-imidazo[4,5-c]pyridin-6-amine (12): ^{1}H NMR (300 MHz, DMSO-d_6, δ ppm): 11.95 (br. s, 1 H), 9.32 (br. s., 2 H), 8.89 (s, 1 H), 8.67 – 8.44 (m, 2 H), 8.15 – 7.76 (m, 4 H), 7.61 (s, 1 H), 7.34 (d, J = 9.0 Hz, 1 H), 3.49 – 3.21 (m, 8 H). ^{13}C NMR (151 MHz, DMSO-d_6, δ ppm): 161.5, 155.1, 152.2, 147.0, 141.2, 136.9, 131.4, 131.1, 130.6, 130.4, 130.2 – 130.0 (br), 128.11, 127.0, 125.1, 124.0, 123.5, 114.2, 46.2, 43.0. LCMS ESI+: found m/z = 440.2 $[M+H]^+$, (calcd for $C_{22}H_{20}F_3N_7$: 439.1732); Purity by LCMS 280nm: 99.7%.

((3S,5R)-3,5-Dimethylpiperazin-1-yl)(2-((2-(4-fluoro-3-(trifluoromethyl)phenyl)-1H-imidazo[4,5-c]pyridin-6-yl)amino)pyridin-4-yl)methanone (35): ^{1}H NMR (300 MHz, DMSO-d6, δ ppm): 8.67 (s, 1H), 8.54 – 8.48 (m, 1H), 8.46 – 8.44 (m, 2H), 8.34 (d, J = 5.1Hz, 1H), 8.03 (s, 1H), 7.59 (t, J = 9.5Hz, 1H), 7.43 (s, 1H), 6.87 (dd, J = 5.2, 1.4 Hz, 1H), 4.73– 4.59 (m, 1H), 3.77 – 3.73 (m, 1H), 3.18 – 3.03 (m, 2H), 3.02 – 2.85(m, 1H), 2.72 – 2.53 (m, 1H), 1.44 – 1.12 (m, 6H). ^{13}C NMR (151 MHz, DMSO-d_6, δ ppm): 167.4, 160.2 (d, $^1J_{C\text{-}F}$ = 260 Hz), 155.5, 150.4, 149.4, 148.2, 145.1, 142.3, 139.5, 137.3, 133.6, 127.2, 125.7, 122.9 (q, $^1J_{C\text{-}F}$ = 275 Hz), 118.8 (d, $^2J_{C\text{-}F}$ = 21 Hz), 118.3 – 117.5 (m),

112.8, 109.1, 93.2, 53.2, 51.4, 50.8, 47.6, 19.0, 18.7. LCMS ESI+: found *m/z* = 515.2 $[M+H]^+$, (calcd for $C_{25}H_{22}F_4N_6O_2$: 514.1740); Purity by LCMS 280nm: 99.7 %.

(2,6-dimethylmorpholino)(2-((2-(4-fluoro-3-(trifluoromethyl)phenyl)-1H-imidazo[4,5-c]pyridin-6-yl)amino)pyridin-4-yl)methanone (36): ^{1}H NMR (300 MHz, Methanol-*d*4, δ ppm): 8.66 (d, *J* = 1.1 Hz, 1H), 8.51 (d, *J* = 6.6 Hz, 1H), 8.44 (dd, *J* = 8.9, 4.9 Hz, 1H), 8.33 (dd, *J* = 5.1, 0.9 Hz, 1H), 8.08 (s, 1H), 7.64 – 7.54 (m, 1H), 7.38 (s, 1H), 6.85 (dd, *J* = 5.2, 1.4 Hz, 1H), 4.51 (d, *J* = 13.5 Hz, 1H), 3.75-3.50 (m, 3H), 2.92 (t, *J* = 11.8 Hz, 1H), 2.60 (t, *J* = 12.0 Hz, 1H), 1.26 (d, *J* = 6.1 Hz, 3H), 1.12 (d, *J* = 6.1 Hz, 3H). ^{13}C NMR (151 MHz, DMSO-d_6, δ ppm): 168.4, 167.5, 161.0 (d, $^1J_{C\text{-}F}$ = 256 Hz), 155.5, 150.6, 149.3, 148.2, 144.8, 139.5, 137.1, 133.7, 127.2, 125.8, 122.9 (q, $^1J_{C\text{-}F}$ = 272 Hz), 118.8 (d, $^2J_{C\text{-}F}$ = 21 Hz), 118.3 – 117.4 (m), 112.8, 109.2, 93.2, 71.9, 71.6, 52.6, 47.1, 19.1, 18.7. LCMS ESI+: found *m/z* = 515.2 $[M+H]^+$, (calcd for $C_{25}H_{22}F_4N_6O_2$: 514.1740); Purity by LCMS 280nm: 99.9%.

4-(tert-Butyl)piperazin-1-yl)(2-((2-(3-(trifluoromethyl)phenyl)-1H-imidazo[4,5-c]pyridin-6-yl)amino)pyridin-4-yl)methanone (39): ^{1}H NMR (300 MHz, DMSO-d_6, δ ppm): 13.29 (s, 1 H), 9.83 (s, 1 H), 8.71 (s, 1 H), 8.55 – 8.41 (m, 2 H), 8.34 – 8.25 (m, 2 H), 7.98 – 7.76 (m, 2 H), 7.46 (s, 1 H), 6.79 (d, *J* = 5.1 Hz, 1 H), 3.74 – 3.48 (m, 2 H), 3.43 – 3.32 (m, 2 H), 2.71 – 2.51 (m, 4 H), 1.07 (s, 9 H). ^{13}C NMR (151 MHz, DMSO-d_6, δ ppm): 167.4, 155.5, 151.1, 149.4, 148.2, 145.1, 142.4, 139.6, 137.4, 131.0, 130.9, 130.7, 130.4 (q, $^2J_{C\text{-}F}$ = 32 Hz), 127.1, 124.4 (q, $^1J_{C\text{-}F}$ = 273 Hz), 123.3, 112.8, 109.2, 93.2, 53.9, 48.1, 46.4, 45.8, 42.5, 26.1. LCMS ESI+: found *m/z* = 524.3 $[M+H]^+$, (calcd for $C_{27}H_{28}F_3N_7O$: 523.2307); Purity by LCMS 280 nm: 98.8%.

(2-((2-(3,4-difluorophenyl)-1H-imidazo[4,5-c]pyridin-6-yl)amino)pyridin-4-yl)(4,4-difluoropiperidin-1-yl)methanone (46): ^{1}H NMR (300 MHz, Methanol -d_4, δ ppm): 8.85 (s, 1H), 8.48 (d, J = 5.5 Hz, 1H), 8.14 (m, 1H), 8.04 (m, 1H), 7.57 (dd, J = 18.2, 8.2 Hz, 1H), 7.51 (s, 1H), 7.21 (s, 1H), 7.19 (d, J = 5.5 Hz, 1H), 3.96-3.88 (m, 2H), 3.62-3.54 (m, 2H), 2.24-2.00 (m, 4H). ^{13}C NMR, HSQC (151 MHz, DMSO-d_6, δ ppm): 146.4, 124.6, 119.2, 116.5, 113.7. 109.6, 44.1, 38.9, 33.9, 33.0. LCMS ESI+: found m/z = 471.2 $[M+H]^+$,(calcd for $C_{23}H_{18}F_4N_6O$: 470.1478); Purity by LCMS: 95 %.

In vitro *P. falciparum* assay:

Compounds were screened against multi-drug resistant (K1) and sensitive (NF54) strains of *P. falciparum* in vitro using the modified [^{3}H]-hypoxanthine incorporation assay[14] and the parasite lactate dehydrogenase assay.[16, 17] Both assays are fully described in the Supporting Information – Section B.

Ethics: For the in vivo pharmacokinetics studies, all animal experiments performed in the manuscript were conducted in compliance with institutional guidelines.

AUTHOR INFORMATION:

Corresponding author

* Phone: +27-21-6502553. Fax: +27-21-650 4521. E-mail: Kelly.Chibale@uct.ac.za

Orcid ID: Kelly Chibale: 0000-0002-1327-4727

ACKNOWLEDGEMENTS: We thank Medicines for Malaria Venture (MMV) and the South African Technology Innovation Agency (TIA) for financial support of this research

(Project MMV09/0002). The University of Cape Town, South African Medical Research Council, and South African Research Chairs Initiative of the Department of Science and Technology, administered through the South African National Research Foundation are gratefully acknowledged for support (K.C). We thank Christoph Fischli, Jolanda Kamber, Sibylle Sax, Christian Scheurer and Ursula Lehmann for assistance in performing antimalarial assays. At UCT, we thank Virgil Verhoog and Sumaya Salie for running the antimalarial assays, Nesia Barnes, Warren Olifant, and Duane Knowles for running the ADME assays, and Trevor Finch for assistance with the animal work. Also, thanks to Marine Barnabe for her help with Figure 2. We thank Matthew Segall, Peter Hunt, and Nick Foster at Optibrium for their assistance with the use of StarDrop.

ABBREVIATIONS USED: ABS, Asexual Blood Stage; ADME, Absorption, Distribution, Metabolism, and Excretion; ADMET, Absorption, Distribution, Metabolism, Excretion and Toxicity; BOC, *tert*-butyloxycarbonyl; CHO cells, Chinese Hamster Ovarian cells; CL, Clearance; CQ, chloroquine; DIPEA, diisopropylethylamine; DMF, dimethylformamide; DMPK, Drug Metabolism and Pharmacokinetics; HATU, 1-[bis(dimethylamino)methylene]-1H-1,2,3-triazolo[4,5-b]pyridinium-3-oxide, hexafluorophosphate; HBD, Hydrogen Bond Donor; hERG, Human Ether-a-go-go-Related Gene; i.v., intravenous administration; LLE, Lipophilic Ligand Efficiancy; MMV, Medicines for Malaria Venture; MW, Molecular Weight; NMR, Nuclear Magnetic Resonance; *P.f.*NSG, *Plasmodium falciparum* NODscidIL2Rγnull; PK, pharmacokinetics; PMB, paramethoxybenzyl; p.o., oral administration; RT, Room Temperature; SAR, Structure-Activity Relationships; TFA, Trifluoroacetic Acid; TPSA,

Topological Polar Surface Area; Vd, Volume of Distribution; WHO, World Health Organization.

ASSOCIATED CONTENT:

Supporting Information Available: Additional details of the characterization of selected compounds and the procedures used for the in vitro assays (antiplasmodial, cytotoxicity, solubility, metabolic stability, hERG inhibition), in vivo PK and metabolism studies, and molecular formula string. This material is available free of charge via the Internet at http://pubs.acs.org.

REFERENCES:

(1) WHO. *Global Technical Strategy for Malaria 2016-2030*; 2015.

(2) WHO. *World Malaria Report 2017*; 2017.

(3) Arie, S. Researchers and WHO Clash over Global Threat of Drug Resistant Malaria. *BMJ* **2017**, *359*, j5127.

(4) Nchinda, A. T.; Le Manach, C.; Paquet, T.; Cabrera, D. G.; Kathryn, J. Identification of Fast-Acting 2 , 6-Disubstituted Imidazopyridines That Are Efficacious in the in Vivo Humanized Plasmodium Falciparum NODscidIL2Rγ Null Mouse Model of Malaria. *J. Med. Chem.* **2018**, *61*, 4213–4227.

(5) Frontrunner template: Late Leads, https://www.mmv.org/research-

development/information-scientists (Accessed Sept 13, 2018).

(6) Bridgland-Taylor, M. H.; Hargreaves, A. C.; Easter, A.; Orme, A.; Henthorn, D. C.; Ding, M.; Davis, A. M.; Small, B. G.; Heapy, C. G.; Abi-Gerges, N.; Persson, F.; Jacobso, I.; Sullivan, M.; Alberstson, N.; Hammond, T. G.; Sullivan, E.; Valentin, J. P.; Pollard, C. E. Optimisation and Validation of a Medium-Throughput Electrophysiology-Based HERG Assay Using IonWorks™ HT. *J. Pharmacol. Toxicol. Methods* **2006**, *54*, 189–199.

(7) Eagle, H.; Musselman, A. D. The Rate of Bactericidal Action of Penicillin in Vitro as a Function of Its Concentration, and Its Paradoxically Reduced Activity at High Concentrations against Certain Organisms. *J. Exp. Med.* **1948**, *88*, 99–131.

(8) Dhingra, S. K.; Redhi, D.; Combrinck, J. M.; Yeo, T.; Okombo, J.; Henrich, P. P.; Cowell, A. N.; Gupta, P.; Stegman, M. L.; Hoke, J. M.; Cooper, R. A.; Winzeler, E.; Mok, S.; Egan, T. J.; Fidock, D. A. A Variant PfCRT Isoform Can Contribute to Plasmodium Falciparum Resistance to the First-Line Partner Drug Piperaquine. *MBio* **2017**, *8*, e00303-17.

(9) Bopp, S.; Magistrado, P.; Wong, W.; Schaffner, S. F.; Mukherjee, A.; Lim, P.; Dhorda, M.; Amaratunga, C.; Woodrow, C. J.; Ashley, E. A.; White, N. J.; Dondorp, A. M.; Fairhurst, R. M.; Ariey, F.; Menard, D.; Wirth, D. F.; Volkman, S. K. Plasmepsin II-III Copy Number Accounts for Bimodal Piperaquine Resistance among Cambodian Plasmodium Falciparum. *Nat. Commun.* **2018**, *9*, 1769–1779.

(10) Mukherjee, A.; Bopp, S.; Magistrado, P.; Wong, W.; Daniels, R.; Demas, A.; Schaffner, S.; Amaratunga, C.; Lim, P.; Dhorda, M.; Miotto, O.; Woodrow, C.; Ashley, E. A.; Dondorp, A. M.; White, N. J.; Wirth, D.; Fairhurst, R.; Volkman, S. K. Artemisinin Resistance without Pfkelch13 Mutations in Plasmodium Falciparum Isolates from Cambodia. *Malar. J.* **2017**, *16*, 1–12.

(11) Ross, L. S.; Dhingra, S. K.; Mok, S.; Yeo, T.; Wicht, K. J.; Kümpornsin, K.; Takala-Harrison, S.; Witkowski, B.; Fairhurst, R. M.; Ariey, F.; Menard, D.; Fidock, D. A. Emerging Southeast Asian PfCRT Mutations Confer Plasmodium Falciparum Resistance to the First-Line Antimalarial Piperaquine. *Nat. Commun.* **2018**, *9*, 3314–3327.

(12) Co, E. M. A.; Dennull, R. A.; Reinbold, D. D.; Waters, N. C.; Johnson, J. D. Assessment of Malaria in Vitro Drug Combination Screening and Mixed-Strain Infections Using the Malaria Sybr Green I-Based Fluorescence Assay. *Antimicrob. Agents Chemother.* **2009**, *53*, 2557–2563.

(13) Patel, V.; Booker, M.; Kramer, M.; Ross, L.; Celatka, C. A.; Kennedy, L. M.; Dvorin, J. D.; Duraisingh, M. T.; Sliz, P.; Wirth, D. F.; Clardy, J. Identification and Characterization of Small Molecule Inhibitors of Plasmodium Falciparum Dihydroorotate Dehydrogenase. *J. Biol. Chem.* **2008**, *283*, 35078–35085.

(14) Snyder, C.; Chollet, J.; Santo-Tomas, J.; Scheurer, C.; Wittlin, S. In Vitro and in Vivo Interaction of Synthetic Peroxide RBx11160 (OZ277) with Piperaquine in Plasmodium Models. *Exp. Parasitol.* **2007**, *115*, 296–300.

(15) www.optibrium.com/stardrop (Accessed Sept 13, 2018).

(16) Desjardins, R. E.; Canfield, C. J.; Haynes, J. D.; Chulay, J. D. Quantitative Assessment of Antimalarial Activity in Vitro by a Semiautomated Microdilution Technique. *Antimicrob. Agents Chemother.* **1979**, *16* (6), 710–718.

(17) Makler, M. T.; Ries, J. M.; Williams, J. A.; Bancroft, J. E.; Piper, R. C.; Gibbins, B. L.; Hinrichs, D. J. Parasite Lactate Dehydrogenase as an Assay for Plasmodium Falciparum Drug Sensitivity. *Am. J. Trop. Med. Hyg.* **1993**, *48* (6), 739–741.

(18) Hopkins, A. L.; Keserü, G. M.; Leeson, P. D.; Rees, D. C.; Reynolds, C. H. The Role of Ligand Efficiency Metrics in Drug Discovery. *Nat. Rev. Drug Discov.* **2014**, *13*, 105–121.

(19) Freeman-Cook, K. D.; Hoffman, R. L.; Johnson, T. W. Lipophilic Efficiency: The Most Important Efficiency Metric in Medicinal Chemistry. *Future Med. Chem.* **2013**, *5*, 113–115.

(20) Hitchcock, S. A. Structural Modifications That Alter the P-Glycoprotein Efflux Properties of Compounds. *J. Med. Chem.* **2012**, *55*, 4877–4895.

(21) Matsson, P.; Doak, B. C.; Over, B.; Kihlberg, J. Cell Permeability beyond the Rule of 5. *Adv. Drug Deliv. Rev.* **2016**, *101*, 42–61.

(22) Kerns, E. H.; Di, L. *Drug-like Properties: Concepts, Structure Design and Methods from ADME to Toxicity Optimization*, Elsevier.; Press, A., Ed.; United States of America, 2008.

Table of contents graphic